



Dynamics of water in LiCl and CaCl₂ aqueous solutions confined in silica matrices: A backscattering neutron spectroscopy study

E. Mamontov^{a,*}, D.R. Cole^b, S. Dai^b, M.D. Pawel^c, C.D. Liang^b, T. Jenkins^{d,e}, G. Gasparovic^{d,e}, E. Kintzel^a

^a Spallation Neutron Source, Oak Ridge National Laboratory, Oak Ridge, TN 37831, United States

^b Chemical Sciences Division, Oak Ridge National Laboratory, Oak Ridge, TN 37831, United States

^c Center for Nanophase Materials Sciences Division, Oak Ridge National Laboratory, Oak Ridge, TN 37831, United States

^d NIST Center for Neutron Research, National Institute of Standards and Technology, Gaithersburg, MD 20899, United States

^e Department of Materials Science and Engineering, University of Maryland, College Park, MD 20742, United States

ARTICLE INFO

Article history:

Received 10 March 2008

Accepted 29 May 2008

Available online 5 June 2008

Keywords:

Water

Confinement

Dynamics

Neutron scattering

ABSTRACT

Backscattering neutron spectroscopy was used to probe the dynamics of water molecules in LiCl and CaCl₂ aqueous solutions confined in 2.7, 1.9, and 1.4 nm diameter pores of various silica matrices. The pore size of 2.7 nm was found to be sufficiently large for the confined liquids to exhibit characteristic traits of bulk behavior, such as a freezing–melting transition and a phase separation. On the other hand, none of the fluids in the 1.4 nm pores exhibited a clear freezing–melting transition; instead, their dynamics at low temperatures gradually became too slow for the nanosecond resolution of the experiment. The greatest suppression of water mobility was observed in the CaCl₂ solutions, which suggests that cation charge and perhaps the cation hydration environment have a profound influence on the dynamics of the water molecules. Quasielastic neutron scattering measurements of pure H₂O and 1 m LiCl–H₂O solution confined in 1.9 nm pores revealed a dynamic transition in both liquids at practically the same temperature of 225–226 K, even though the dynamics of the solution at room temperature appeared to slow down by more than an order of magnitude compared to the pure water. The observation of the dynamic transition in the solution suggests that this transition may be a universal feature of water governed by processes acting on the local scale, such as a change in the hydrogen bonding.

© 2008 Elsevier B.V. All rights reserved.

1. Introduction

Although aqueous solutions in confined environments play a prominent role in various processes, to date it has been almost exclusively pure water and, less often, non-polar fluids that have attracted attention in research of confined liquids. Neutron scattering has been employed extensively for investigating structural and dynamic properties of confined water. In particular, dynamics of confined water can be readily probed by neutron scattering due to the large incoherent scattering cross-section of hydrogen. Quasi-elastic neutron scattering (QENS) is often a technique of choice for studying mobility of hydrogen-containing species and has been used in numerous studies of confined water. On the other hand, there have been few QENS studies of aqueous solutions in the bulk form [1–5] and almost none in confinement [6,7]. The relative lack of QENS studies of aqueous solutions could possibly be attributed to the fact that even the dynamic properties of pure water, which represents the limiting case of an infinitely dilute solution, are not well understood, while the presence of ions adds another layer of

complexity [8]. Nevertheless, in natural and engineered confining systems, water rarely remains pure but instead can incorporate solutes due to interactions with confining matrices. Thus, there are compelling reasons to carry out experiments aimed at comparing properties of pure water and aqueous solutions in the same confining environment, even if theoretical understanding of confined water and solutions may be far from complete. In this work, we have investigated the effect of adding salts on the diffusion dynamics on the nanosecond time scale of water confined in silica matrices with pores of various sizes. Silica is a typical example of a hydrophilic material and, as such, is representative of the entire class of oxide-based confined matrices important in various technological applications and in earth science.

We have employed backscattering neutron spectroscopy to investigate the dynamics of LiCl and CaCl₂ aqueous solutions confined in silica pores with a diameter of 2.7, 1.9, and 1.4 nm at ambient temperature and below. Comparative analysis of the fluid dynamics in the largest and smallest pores has been performed using elastic intensity scan technique. While the liquids in the largest pores that we probed exhibit freezing–melting transitions in a range of temperatures below 230 K, those confined in the smaller pores do not freeze and retain mobility on the nanosecond time

* Corresponding author.

E-mail address: mamontove@ornl.gov (E. Mamontov).

scale down to at least 190 K. The intermediate pore size of 1.9 nm has been chosen for the more detailed QENS analysis of the confined fluid dynamics. In agreement with the results of our previous study of Vycor glass-confined fluids [7], the combined effects of confinement and adding a salt was found to suppress the mobility of water to a much greater extent (by at least an order of magnitude) than one would expect from either confining pure water or from a solution in the bulk form. We have observed a dynamic transition in a confined LiCl–H₂O solution, between about 230 and 220 K, similar to the one exhibited by pure water in the same confining environment. Since adding a salt to confined water results in even more restrictive confinement experienced by the free molecules outside the ion hydration shells, our findings suggest that the dynamic transition in water may be associated with processes acting on a local scale, such as, for instance, a change in the hydrogen bonding that occurs near the temperature of the transition.

2. Experiment

2.1. Initial materials

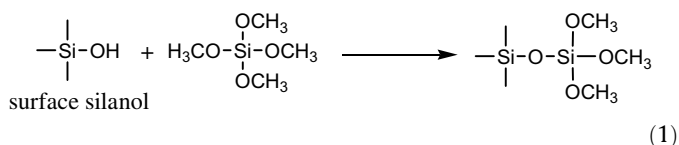
Commercially available MCM41 mesoporous silica (CAS Number 112945-52-5) with an average pore size of 2.7 nm (BJH) was purchased from Sigma–Aldrich and used without further modification. Anhydrous toluene 99.8% (ACROS, 61046-0010, CAS Number 108-88-3), methanol, HPLC grade (Burdick and Jackson, AH230-4, CAS Number 67-56-1), nitric acid, 68–70% (VWR, VW4815-6, CAS Number 7697-37-2), hydrochloric acid, 36.5–38% (VWR, VW3110-3, CAS Number 7647-01-0), pluronic F127 (Sigma, P2443-250 G, CAS Number 9003-11-6), and 1-butanol HPLC grade (Fisher, A383SK-4, CAS Number 71-36-3) were used as received. Tetramethyl orthosilicate (TMOS) 98+% (Aldrich, 679259-50G, CAS Number 681-84-5) was redistilled prior to use. Deionized (DI) water was homemade by a Millipore water purification system. The acids were diluted to the concentrations specified in the synthesis by using homemade DI water.

2.2. Surface sol–gel modification of MCM41

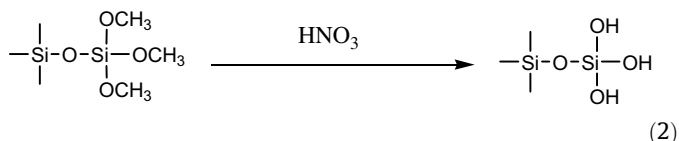
Commercial MCM41 was modified using the surface sol–gel (SSG) technique [9] to obtain an average pore size of 1.9 nm. The SSG process enables the molecular-scale control of film thickness over a large 2D substrate area and can be viewed as a solution-based methodology for atomic layer deposition (ALD) synthesis. The SSG technique generally consists of two half reactions: (i) non-aqueous condensation of alkoxide precursor molecules with surface hydroxyl groups and (ii) aqueous hydrolysis of the adsorbed alkoxide species to regenerate surface hydroxyls. The iteration of the above sequential condensation and hydrolysis reactions allows the layer-by-layer coating of a selected oxide on a hydroxyl-terminated surface. Although the original technique was developed to functionalize 2D surfaces, we have recently applied the SSG process to the surface modification of both porous and nonporous silica materials as well as titanium-oxide nanocrystals with various tailored oxide thin films for catalysis applications [10–12].

Four complete cycles of the SSG process were conducted on the commercial MCM41 to reduce the pore size to 1.9 nm. Each cycle of the SSG process contains two consecutive steps. The first step was the generation of surface silanol groups. MCM41 (20 g) was refluxed in 10% nitric acid for 2 h and then washed with a copious amount of DI water. The solid sample was dried under vacuum for 4 h at 120 °C. The second step was the addition of a new layer of silica through the SSG process. Firstly, the surface-hydrolyzed sample was mixed with 500 mL of anhydrous toluene and 4.5 mL

of TMOS under a stream of dry nitrogen. The mixture was heated to reflux for 2 h to ensure the completion of the SSG reaction:



Subsequently, the solid sample was collected by filtration and washed thoroughly with methanol to remove the excess TMOS. Except for the first cycle, the generation of surface silanol groups via hydrolysis followed the reaction:



After the completion of the fourth cycle, the surface of the modified MCM41 was hydrolyzed to silanol groups by the repetition of step 1. The resultant MCM41 is denoted as MCM41*. It should be noted that both MCM41 and MCM41* possess arrays of long, non-interconnecting, cylindrical pores.

2.3. Synthesis of sintered SBA15

The sintered SBA15 was synthesized using a modified procedure reported by Stucky and co-workers [13]. Briefly, a colloidal silica solution was first prepared by mixing TMOS (22.9 g) with 0.01 mol/L HCl (15.8 g) and stirring for 1 h. A mixture of F127 (10 g) and 1-butanol (4.28 g) was then added to the colloidal silica solution. The mixture was stirred until the solids were completely dissolved. Afterwards, the solution was sealed in a plastic bottle and heated at 100 °C for 12 h. The bottle was then opened to dry the solution in a well-vented hood. The residual methanol from the hydrolysis was completely removed under vacuum. The organic species was decomposed by slowly heating the monolith in air with a ramp of 1 °C/min from room temperature to 850 °C. The resultant product was further calcined at 850 °C for additional 40 h to form a microporous material with an average particle size of a few millimeters. The sintering of the SBA15 sample caused the collapse of the mesoporous channels, leaving mostly micropores (less than 1.8 nm in diameter, 1.4 nm on average) accessible for hydration. This “mesopore-collapsed” SBA15 is denoted as SBA15*.

2.4. N₂ adsorption measurements

The pore sizes of three porous silicate samples were measured by a Quantachrome Autosorb-II through nitrogen adsorption and desorption at 77 K. The calculation of pore-size distributions was based on the corresponding adsorption isotherms. Although several theories can be used to calculate pore sizes, there is no universal method for the calculation of pore sizes in all range of pore sizes [14]. Barrett–Joyner–Halenda (BJH) method is widely accepted for calculating pore sizes in the range of 1.8–50 nm. Density function theory (DFT) is generally used for the calculation of micropores. For a fair comparison of the pore size distributions (PSD's), the BJH method was employed to calculate PSD's for the MCM41 and MCM41* samples while the DFT method was used for the SBA15* sample. Fig. 1 shows the PSD's of MCM41, MCM41*, and SBA15* samples.

2.5. Hydration

For this study, we selected lithium chloride and calcium chloride solutions because these are salts commonly found in natural

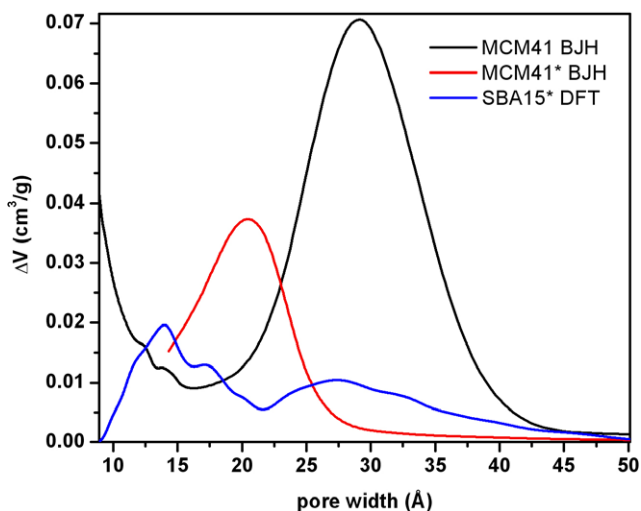


Fig. 1. Pore-size distributions of three silicates: MCM41, MCM41*, and SBA15*. Note: the pore-size distributions of MCM41 and MCM41* were calculated by BJH method, and the pore-size distribution of SBA15* by DFT method.

and engineered systems and because an early QENS study of the bulk solutions [2] indicated that Ca^{2+} - H_2O and Li^+ - H_2O subsystems are in the fast exchange limit. The latter means that the binding time of the first hydration shell to the cation is short compared to the characteristic observation time of the neutron scattering event (about a nanosecond in a neutron backscattering experiment). Thus, during this observation time a water molecule experiences the entire range of environments present in the solution [2]. In turn, this allows for a more straightforward interpretation of the QENS data.

Pure salts (both at 99.99%) of LiCl and $\text{CaCl}_2 \cdot 6\text{H}_2\text{O}$ were obtained from Ultra Scientific; Lot Nos. E00417 and E00454, respectively. Starting stock solutions of concentrated LiCl and CaCl_2 were made by adding these salts in distilled water purged with argon for ~ 30 min. More dilute concentrations at the desired molalities (1 and 4 for LiCl and 0.667 and 1.333 for CaCl_2) were then made by simple dilution of the more concentrated stock solutions using the same purged pure water. The three types of silica samples were hydrated by soaking roughly 2 g of each powder in approximately 10 g of each solution (pure water and the various salt solutions of LiCl or CaCl_2) for roughly 48 h. This duration was sufficient to allow for complete saturation of the pores as well as to allow for the powders to settle such that the overlying excess solution could be decanted off leaving behind thick paste-like slurry of hydrated material. It was determined that different drying times (in near-zero humidity dry air) were needed to remove excess bulk (external) water from powders but still leave the pores fully saturated; 8–10 h for silica–pure water, 16–18 h for silica–LiCl and 48 h for silica– CaCl_2 . The hygroscopic nature of CaCl_2 proved problematic so the drying step for the silica– CaCl_2 powders was timed so that at the end of the 48 h, powder was quickly (< 10 min) removed from the drying environment and loaded into the cell before appreciable external rehydration could take place.

2.6. Neutron scattering experiments

The thickness of the samples of 1 mm was chosen to ensure greater than 90% neutron transmission through the sample in order to minimize effects due to multiple scattering of neutrons in the samples. The aluminum sample containers were sealed with indium O-rings and mounted onto a top-loading closed-cycle refrigerator that used a helium exchange gas to cool the samples, thus minimizing the temperature gradient through the samples.

The top-loading closed-cycle refrigerator that we used provides temperature stability of 1 K or better.

Neutron scattering experiments were performed at the National Institute of Standards and Technology (NIST) Center for Neutron Research (NCNR) using the high flux backscattering spectrometer (HFBS) [15]. On the HFBS, the incident neutron wavelength is varied via Doppler selection about a nominal value of 6.271 Å ($E_0 = 2.08$ meV). After scattering from the sample, only neutrons having a fixed final energy of 2.08 meV are measured by the detectors as ensured by Bragg reflection from Si(1 1 1) analyzer crystals. The difference between the variable incident energy and fixed final energy yields the value of neutron energy transfer in QENS studies. Alternatively, the Doppler-driven monochromator can be stopped, thereby fixing the incident energy at 2.08 meV, which ensures that all the detected neutrons were scattered without energy transfer (that is, elastically), within the accuracy of the energy resolution of the spectrometer. The scattering intensities obtained in this way are measured as a function of an external parameter, which is typically the sample temperature. This mode of operation, usually called elastic intensity on fixed-window scans, provides a time-effective way to evaluate the dynamics of a sample over a wide temperature range. Most of our samples were studied using elastic intensity temperature scans with a temperature ramp rate of 1 K/min (cooling down). For the QENS studies of two selected samples, the HFBS was operated with a dynamic range of ± 11 μeV to provide the best energy resolution and the highest neutron counting rates. With this dynamic range, the spectrometer resolution function had a full width at half-maximum (FWHM) of 0.85 μeV , as we determined from the low-temperature data. Due to the overwhelmingly strong small-angle elastic scattering from the silica materials, the low-angle detectors had to be excluded from the analysis of data. Thus, we used the data collected for the scattering momentum transfers of $0.62 \text{ \AA}^{-1} < Q < 1.68 \text{ \AA}^{-1}$ (at the elastic channel). The data were summed up over the entire Q range, as we will explain below.

3. Results and discussion

In the Q -range selected for the data analysis, the scattering intensity from our samples is dominated by the signal from hydrogen atoms in confined water due to the large incoherent scattering cross-section of hydrogen. Since our initial goal was to compare the dynamics of water molecules in solutions of different salts at various concentrations in pores of different size at as many temperatures as possible, we were presented with a task of carrying out a series of temperature-dependent neutron scattering measurements on a number of samples. We have accomplished this by means of employing elastic intensity scans as a function of sample temperature, which allowed measuring ten samples in four days. The high throughput of elastic scans is achieved at the expense of integrating information about the dynamics on various time scales, which is only available from full dynamic measurement. For comparison, the same neutron beam time of four days was later required to carry out full dynamic QENS measurements of just two samples.

3.1. Elastic intensity scans

The elastic intensity scans spanned a temperature range of 5–325 K. At temperatures higher than the baseline temperature of the scan (about 5 K), the intensity invariably decreases due to Debye–Waller thermal factors. This is because a certain fraction of the elastic scattering intensity, which increases with temperature, becomes redistributed to the inelastic (vibrational) channels. If there are no species in the sample that become mobile on the time

scale of the spectrometer resolution within the temperature range scanned, then the elastic intensity monotonically decreases at higher temperatures, as exemplified by the dry MCM41 sample. Actually, even the dry MCM41 spectrum shows some small nonlinearity which is likely associated with a small residual amount of water, whereas the “dry” SBA15⁺ spectrum exhibits somewhat more significant nonlinearity indicative of incomplete dehydration.

In the presence of species that become mobile, either due to a freezing–melting transition or because their diffusion dynamics become faster than the spectrometer resolution (a few nanoseconds), there is a significant reduction in the elastic intensity in addition to the normal Debye–Waller behavior. This is because, in addition to the redistribution of the elastic intensity to the vibrational channels, there is a very significant redistribution to the quasielastic scattering channels. In a QENS measurement, the latter redistribution would manifest itself as wings of the QENS signal that develop at the expense of the elastic peak. At higher temperatures, the intensity of the QENS scattering increases, whereas the intensity of the elastic signal (in both QENS and elastic scan measurements) decreases, due to the overall increased water mobility in the system. However, at even higher temperatures the fraction of species mobile on the time scale of the spectrometer resolution eventually becomes saturated, and the elastic scattering intensity regains the Debye–Waller behavior, again starting exhibiting a monotonic decrease with increasing temperature. Based on the elastic intensity scans, it is sometimes possible to differentiate between a sharper freezing–melting transition and a gradual change in the mobility the system, when the dynamics eventually becomes too slow for the experiment time resolution. In the limiting case of a freezing–melting bulk liquid, the transition is well defined and manifests itself as a prominent and abrupt step in the elastic intensity scan.

All the hydrated samples in our measurements exhibit the onset of diffusion dynamics within the temperature range of the elastic scans of 5–325 K (Fig. 2). The MCM41 sample with H₂O in the 2.7 nm pores shows rather sharp transition at about 230 K that we attribute to water freezing in the pores. This value is in good agreement with the data available in the literature. For example, the following freezing temperatures have been reported for water confined in various silica matrices: 252 K and 237 K in silica with the average pore size of 10 nm and 3 nm, respectively [16], 260 K in 9 nm silica pores [17], 242 K and 221 K in 1.87 nm and 1.44 nm MCM41 [18], 232 K in 4.2 nm MCM41 [19], and 255 K in Vycor glass with the average pore size of 5 nm [20]. In general, a greater suppression of the freezing point of confined water is associated with smaller pore sizes.

Both 0.67 mol/L and 1.33 mol/L CaCl₂–H₂O solutions in MCM41 exhibit somewhat less well-defined transitions at temperatures lower by 10–15 K compared to the MCM41-confined H₂O. Both of these solutions, especially the more concentrated 1.33 m CaCl₂–H₂O, show kinks in the elastic intensity near the transition temperature. These are indicative of phase separation and subsequent freezing of certain phases, while the other confined phases still retain mobility. Such phase separation is in agreement with the phase diagram of the CaCl₂–H₂O system [21], although its temperature measured in our experiment in confinement is lowered compared to the solution in bulk form. Compared to the MCM41-confined calcium chloride solutions, the MCM41-confined lithium chloride solution shows a smoother transition with no obvious features, making it difficult to assign unambiguously to either gradual freezing of the solution or gradual slowing down the dynamics below the resolution limit of the HFBS. In summary, adding salts to water confined in 2.7 nm pores further suppresses the temperature of the freezing transition which is already suppressed by confinement. A pore size of 2.7 nm is sufficiently large for the confined liquids to exhibit characteristic traits of bulk behavior, such as a

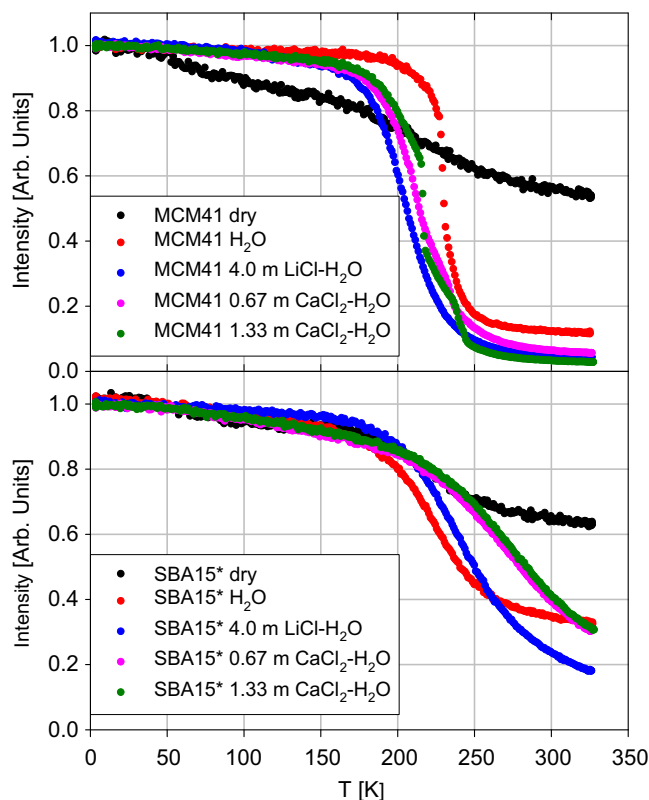


Fig. 2. The results of the HFBS neutron elastic scattering intensity scans summed up for $0.62 \text{ \AA}^{-1} < Q < 1.68 \text{ \AA}^{-1}$ for water and solutions confined in MCM41 and SBA15⁺. The spectra have been normalized to the intensities measured at 5 K.

freezing–melting transition and a phase separation. Above about 250 K, all water molecules in the fluids confined in 2.7 nm pores become mobile on the time scale faster than a nanosecond, as evidenced by the elastic scan intensities that return to the Debye–Waller decay.

The dynamics of liquids confined in the 1.4 nm pores of the SBA15⁺ sample show very different behavior. Pure SBA15⁺-confined H₂O does not show a freezing–melting transition similar to the one exhibited by MCM41-confined H₂O; instead it exhibits a gradual slowing down of the dynamics down to the temperatures below 200 K, where eventually it becomes too slow for the HFBS resolution. On the high-temperature end of the spectrum, all the water molecules in this pure water system become mobile on the time scale faster than a nanosecond at about room temperature, as evidenced by the end of a rapid decrease in the elastic scan intensity and its return to the Debye–Waller decay. The calcium chloride and lithium chloride solutions exhibit qualitatively similar behavior, but their dynamics slow down substantially compared to pure H₂O. This is evidenced by the following observations. First, unlike that of pure water, the aqueous solution mobilities become too slow for the HFBS resolution (as evidenced by entering the Debye–Waller regime) not below, but above 200 K. Second, even at the highest temperature of the measurements, 325 K, the elastic scans of the solutions, unlike that of pure water, still show an ongoing transition, not a Debye–Waller decay, indicating that more water molecules could become mobile at higher temperatures. The extent to which the dynamics slow down seems to be dependent more on the charge of the cations in solution than on the solution ionic strength. While the 4 m LiCl–H₂O solution shows a moderate slowing down compared to pure H₂O, the 1.33 m CaCl₂–H₂O solution of the same ionic strength exhibits substantially slower mobility, similar to that of the 0.67 m CaCl₂–H₂O solution, which is at half of the ionic strength of the lithium chloride solution.

3.2. QENS measurements

For QENS studies, we selected a 1 m LiCl–H₂O solution and pure H₂O (as a reference sample) confined in 1.9 nm pores on MCM41*. Our goal was to use a confining matrix with the pore size as large as possible to minimize the influence of the pore walls, but small enough to completely suppress the freezing transition. While the lithium chloride solution in the 2.7 nm pores of the unmodified MCM41 may or may not freeze, pure water in the 2.7 nm pores does freeze (see Fig. 2). Thus, using a confinement size of 2.7 nm would preclude comparison of the water and solution dynamics in the same matrix at low temperatures. In addition to the intermediate pore size (leading presumably to less influence from the pore walls), another advantageous feature of the MCM41* compared to the SBA15* is a much more uniform pore size distribution.

The dynamic spectra of 1 m LiCl–H₂O solution and pure H₂O in MCM41* are shown in Fig. 3, where the 5 K data represent the resolution of the experiment. As we have mentioned above, the data were summed up over the entire Q range of the measurement from $0.62 \text{ \AA}^{-1} < Q < 1.68 \text{ \AA}^{-1}$. This is possible because of the localized nature of the translational diffusion process in the systems that we study (on the length scale much smaller than the confining pore size), which leads to a weak Q -dependence of the QENS broadening even at high temperatures, as we have demonstrated in the previous work [7]. The results presented in Fig. 3 indicate a gradual change in the QENS signal as a function of temperature for confined lithium chloride, whereas the QENS signal from the confined pure water is much more temperature-dependent and rapidly becomes

too broad for the dynamic range of the measurement at higher temperatures. We fit the experimental data using the expression

$$I(E) = [\chi\delta(E) + (1 - \chi)S(E) + (BE + C)] \otimes R(E) \quad (3)$$

Here $\delta(E)$ is a delta function centered at zero energy transfer, χ represents the fraction of the elastic scattering in the signal, the linear term $(BE + C)$ describes the inelastic background and the contribution from fast rotational diffusion, $R(E)$ is the resolution function, and $S(E)$ is the model scattering function describing the functional dependence of the QENS signal. As the scattering from silica matrix is very weak, the elastic signal described by the parameter χ originates predominantly from the scattering by immobile (on the time scale of the measurement) water species, such as the water molecules in direct contact with the pore walls. Another significant source of the elastic scattering may be the silanol groups on the inner silica surface. Additionally, there may be a significant contribution to the elastic signal from the water of hydration surrounding the ions, provided that the latter are stable on the time scale of the measurement, as we will discuss below.

Our estimates of the contribution to the measured scattering intensity from various types of hydrogen atoms in the samples are as follows. For the pure H₂O sample, about 25% of the scattering signal originates from the silanol groups, and about 38% from the water in direct contact with the pore walls. Thus, about 37% of the scattering intensity originates from the water molecules that are mobile on the nanosecond time scale. It should be noted that the experimentally observed fraction of the elastic scattering is greater than 63%, as the scattering from the mobile water molecules is both quasielastic and elastic due to the restricted character of the translational diffusion process [7]. Likewise, for the 1 m LiCl–H₂O sample, about 37% of the scattering signal originates from the water molecules that are not in direct contact with the pore walls. These include both the “free” water molecules (outside the first ion hydration shells) and the water molecules in the first hydration shells. Assuming coordination numbers of 4 and 6 for Li⁺ and Cl[−], respectively, one can conclude that about 30% of the total scattering signal originates from the “free” water molecules, and about 7% from the hydration shell water molecules. Whether the scattering from the latter water molecules is completely elastic on the time scale of the experiment or not, depends on how fast they exchange with the “free” water molecules. As we discuss below, there is a possibility that the hydration water molecules are not in the fast exchange limit (on the nanosecond time scale of the experiment). Thus, we investigated the effect of aqueous LiCl on the spatially restricted translational diffusive motions of the “free” water molecules (and, possibly, the water molecules in the ion hydration shells, if the latter are in the fast exchange limit) on the nanosecond time scale.

We used the model scattering function in the form of a Fourier transform of a stretched exponential:

$$S(E) = A \int_0^\infty \exp\left[-\left(\frac{t}{\tau}\right)^\beta\right] \exp\left(i\frac{E}{\hbar}t\right) dt \quad (4)$$

where A is a scaling constant, and $0 < \beta < 1$. Based on the fit parameters τ and β , the average relaxation time can be calculated as $\langle\tau\rangle = (\tau/\beta)\Gamma(1/\beta)$, where Γ is the gamma-function. This functional form is by no means unique: it is just one way to extract average relaxation times for the system with complex dynamics, such as confined liquids.

3.3. Temperature dependence of the relaxation times

The temperature dependence of the average relaxation times is shown in Fig. 4. The reference H₂O sample exhibits temperature dependence typical of confined water. Down to about 225 K, the relaxation times rapidly increase as the temperature is decreased,

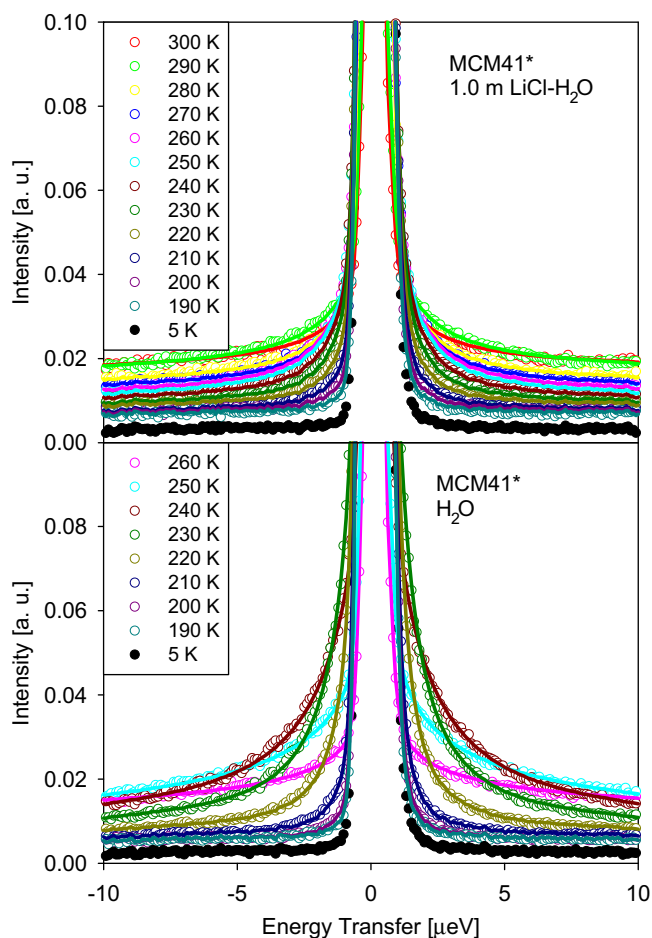


Fig. 3. Symbols: the scattering intensities collected on the HFBS for water and solution confined in MCM41*. The data were summed up for $0.62 \text{ \AA}^{-1} < Q < 1.68 \text{ \AA}^{-1}$. Solid lines: fits obtained using Eqs. (3) and (4).

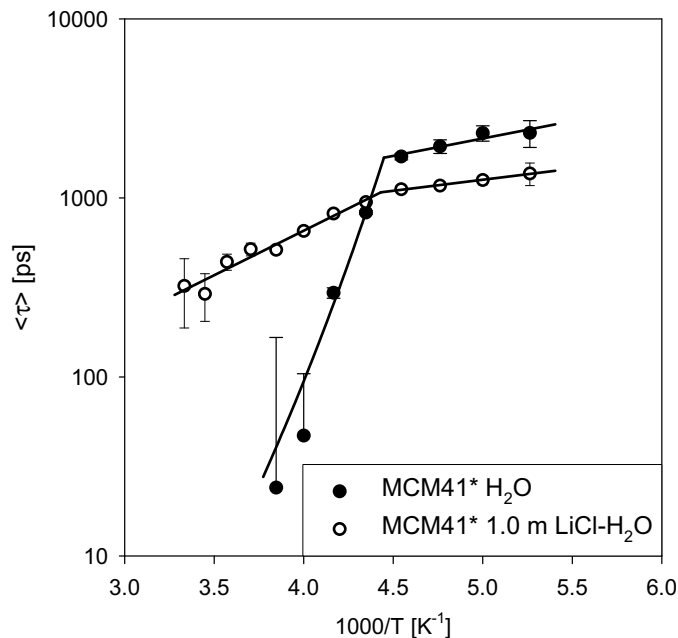


Fig. 4. The average relaxation times as a function of inverse temperature obtained from the fits of the HFBS data shown in Fig. 3 as $\langle \tau \rangle = (\tau/\beta)\Gamma(1/\beta)$, where Γ is the gamma-function (error bars represent a standard deviation). Shown as solid lines are a VFT and an Arrhenius fit for confined water and Arrhenius fits for confined solution.

and we can fit the temperature points of 260, 250, 240, and 230 K using a Vogel–Fulcher–Tammann (VFT) law, $\tau = \tau_0 \exp(DT_0/(T - T_0))$, with a Vogel temperature $T_0 = 122$ K. The dimensionless fit parameter D is not related to the diffusion coefficient. It should be noted that the relaxation times for water measured at 260 K and 250 K have very large error bars because the QENS signal at these temperatures becomes too broad for the ± 11 μ eV dynamic range of the experiment, as one can see in Fig. 3. Nevertheless, even though the temperature dependence for pure H₂O at higher temperatures can be determined only qualitatively, one can definitely see a transition to a different dynamic regime at 225 K, below which the H₂O relaxation times exhibits an Arrhenius temperature dependence with an activation energy of 3.7 kJ/mol. Remarkably, the dynamics of the lithium chloride solution show a transition at a very similar temperature of 226 K. Below this temperature, its relaxation times demonstrate an Arrhenius temperature dependence with an activation energy of 2.4 kJ/mol. In the temperature range of 230–300 K, the relaxation times observed for the confined solution can be fit with another Arrhenius law with much higher activation energy of 9.5 kJ/mol. While a VFT model may not constrain the data for the confined solutions above 230 K as well as an Arrhenius fit, the presence of a dynamic transition between 230 and 220 K is clear. Furthermore, the fact that a dynamic transition occurs in both systems at practically the same temperature but at significantly different relaxation times demonstrates that the observed transition is unlikely to be an artifact due to the spectrometer resolution, as one could argue in the absence of the LiCl–H₂O data.

We observe that the combined effect of confinement and adding a salt dramatically increases the relaxation time for the water molecules in the confined solution, to a much greater extent compared to bulk liquids. This is in agreement with our earlier experiments on liquids confined in Vycor glass [7]. For example, the diffusion coefficient measured by QENS for water in a 5 m LiCl–H₂O solution in the bulk form, where there were about 11 H₂O molecules per 1 molecule of LiCl, was 13×10^{-10} m²/s, or about 57% of the value for pure bulk water [2]. In a much more dilute 1 m LiCl–H₂O solution that we used in the current study there are about 55 H₂O mole-

cules per 1 molecule of LiCl. Thus, we can expect even smaller decrease of the diffusion coefficient compared to pure water for this solution in the bulk form. However, as one can see in Fig. 4, for these liquids in confinement, the average relaxation times at temperatures above the dynamic transition are very different, showing a difference of more than an order of magnitude near the room temperature. Therefore, the data in Fig. 4 are indicative of a very significant difference in the diffusivities between the confined water and 1 m LiCl–H₂O solution.

3.4. Effects of ion hydration and confinement on dynamics

Even though the LiCl solution is fairly dilute, the solvated ions appear to exert a significant influence on the dynamics of the water molecules in the system. A possible explanation that we have proposed in the earlier study [7] is that confinement in small pores may promote stabilization of the Li⁺– n H₂O (n up to 4) and possibly Cl[−]– n H₂O (n up to 6) hydration complexes on the time scale of the neutron backscattering measurement (from hundreds of picoseconds to above a nanosecond). There is a possibility that confinement in the small pores may have a much stronger effect on the dynamics of hydration complexes, which are significantly larger in size compared to individual water molecules. This may lead to stabilization of the hydration shells. If true, this would imply that, unlike in bulk solutions, the ion–water hydration complexes in the confined solutions are no longer in the fast exchange limit. Instead, the binding time of the first hydration shell water molecules becomes long compared to the characteristic time scale of the neutron backscattering measurement. The implication of the stabilization of the hydration complexes for the diffusion dynamics of the free water molecules observed in the QENS experiment is that free water may experience a confining volume that is much smaller than the pore size, which may explain a dramatic slowing down of their diffusion dynamics. On the other hand, in bulk solutions the hydration complexes are unstable on the time scale of the neutron measurement (fast exchange limit), and the dynamics of the water molecules is only slightly affected by the presence of salt. Thus, adding a salt to water and confining it in small pores may have a synergetic effect on the free water dynamics.

It should be noted that suppression of translational water dynamics via “chemical confinement” in the molecular solutions has been commonly observed in chemical mixtures [22,23] and concentrated solutions of biomolecules [24–27]. One interesting example was a study of a dimethyl-sulfoxide/water mixture [22] where self-diffusion coefficient and the residence time between jumps for water molecules became Arrhenius, in contrast to non-Arrhenius behavior in pure water. This is similar to our results on the residence times in the lithium chloride solution that exhibit an Arrhenius behavior (see Fig. 4). However, due to confinement of the solution in silica, we were able to investigate the dynamics down to much lower temperatures, which allowed observation of a dynamic transition.

Another mechanism that may contribute to the slowing down of water dynamics is the interaction between either free water and/or hydration sphere water molecules with the silica pore walls. It is well known that when water interacts with the SiO₂ surface, the water molecule may dissociate, with the hydroxide bonding to Si atoms to form silanol (Si–OH) surface sites and the proton bonding to either surface oxygen atoms thus forming silanols or to bridging oxygen atoms [28]. The specific features of how ionic hydration waters interact with an oxide surface is not so well understood. However, based on recent work detailing the adsorption of divalent cations (e.g. Sr, Rb, Ba) in chloride media to titanium oxide [29,30] or mica [31] surfaces one can envision the potential for hydration (inner and/or outer) sphere water hydrogens linking up to varying degree with the surface oxygen atoms

or unsatisfied siloxane (Si–O) oxygen atoms. Thus the combination of ionic hydration, restricted mobility dependent on pore size and water–silica interfacial interactions may act in concert to reduce water dynamics in a profound manner.

3.5. Dynamic transition in confined liquids

The presence of a dynamic transition in water in a confined LiCl–H₂O solution is perhaps the most interesting result of these experiments. The fact that the transition is present in the system where the water molecules experience a much higher degree of confinement compared to the molecules of pure water in pores of the same size suggest that the transition may be associated with processes acting on a local scale. While the dynamic transition seems to be a common feature of water confined in various systems [32–39] its mechanism remains a hotly debated topic. The original explanation supported by molecular dynamics (MD) simulations [40], is that the crossover in the water dynamics represents the “fragile”-to-“strong” liquid transition predicted a decade ago [41]. In this interpretation, the dynamic transition reflects the structural changes due to a transformation from a high-density, high-temperature, liquid phase to a low-density, low-temperature, liquid phase having a much more well-developed hydrogen bond network. It has been also argued that the observed dynamic transition could be due to a confinement-induced vanishing of the α -relaxation in water, which leaves only a β -relaxation that is characterized by Arrhenius behavior [42]. Arguments in favor of an Arrhenius behavior of β -relaxation related to the dynamics of hydrogen bonds were given in [43]. More recently, the possible role of nano-confinement in inducing the dynamics transition was questioned due to the fact that the transition has been always observed in nano-confined water, with confining surfaces composed of amorphous silica and other discrete molecular phases [44,45]. It is possible that in both confined pure water and aqueous solution the change of dynamics observed between 220 K and 230 K is accompanied by the change of population of different types of hydrogen atoms (for example, through increasing number of immobile or slow moving water molecules). Even in such case, the change in the diffusion dynamics of the water molecules is still involved. A possible role of the dynamic transition in the hydration water in the dynamic transition in hydrated biomolecules is also an actively debated topic [36,37,46,47].

In our confined LiCl–H₂O solution, the molecules of the ion hydration shells appear to play the role of a major confining medium for the free water molecules, judging by the extent by which the dynamics of free water in the confined solution is suppressed compared to the confined pure H₂O. This suggests that the transition may be an universal feature governed by intrinsic properties of water that change at about the transition temperature, even though this temperature may depend significantly on the confining matrix [39]. In particular, there is a possibility that the transition is associated with a change in hydrogen bonding. In this regard, an interesting recent study [48] of heat capacity and vibrational density of states of water in contact with an oxide surface (anatase polymorph of TiO₂) has shown that the heat capacity of the confined water falls below that of bulk ice below some 200 K. The heat capacity of the confined water above this temperature exceeds that of bulk ice, possibly indicating the existence of additional vibrational degrees of freedom above the temperature close to the temperature of the dynamic transition.

4. Conclusion

We have studied the dynamics of pure water and lithium chloride and calcium chloride aqueous solutions confined in the pores

of silica matrices using backscattering neutron spectroscopy. In the 2.7 nm pores, pure water freezes at about 230 K, in agreement with the data available in the literature. The confined solutions of calcium chloride show evidence of phase separation. Both lithium chloride and calcium chloride solutions in the 2.7 nm pores freeze at temperatures below that of pure confined water freezing. We conclude that a pore size of 2.7 nm is sufficiently large for the confined liquids to exhibit characteristic traits of bulk behavior, such as a freezing–melting transition and a phase separation. In the smallest pores examined of 1.4 nm, none of the fluids in our experiment exhibit a clear freezing–melting transition. Instead, their dynamics at low temperatures gradually become too slow for the nanosecond resolution of the measurement. In contrast with the liquids in the largest pores, some water molecules in the solutions confined in the 1.4 nm pores are still not mobile on the nanosecond time scale at the highest temperature of the experiment of 325 K, indicating substantial slowing down of the dynamics in the small pores. The cation charge, and by extension, the hydration environment (Ca²⁺ vs. Li⁺) appear to have much greater effect on the dynamics than the ionic strength of the solutions, leading to slower dynamics for the calcium chloride solutions. Comparative QENS measurements of pure H₂O and 1 m LiCl–H₂O solution confined in 1.9 nm pores show a dynamic transition in both liquids at practically the same temperature of 225–226 K. At the same time, the dynamics of the confined lithium chloride solution at room temperature slows down by more than an order of magnitude compared to the confined pure water. This finding demonstrates that the cumulative effect of adding a salt to water in confinement on the mobility of the water molecules is much greater than one would expect from either confining water or forming a solution in the bulk form. This is also in agreement with our earlier experiment [7] on the dynamics of fluids confined in larger (5 nm) pores of Vycor glass. Finally, our observation of the dynamic transition in a solution suggests that this transition may be a universal feature of water governed by its intrinsic properties that act on the local scale, such as hydrogen bonding.

Acknowledgements

The authors are thankful to M. Zamponi and J. Rosenqvist for critical reading of the manuscript. This work utilized NCNR neutron scattering facilities supported in part by the National Science Foundation under Agreement No. DMR-0454672. The synthesis and characterization of the porous silicates were conducted at the Center for Nanophase Materials Sciences, which is sponsored at Oak Ridge National Laboratory by the Scientific User Facilities Division, Office of Basic Energy Sciences, US Department of Energy. This work was sponsored in part by the Laboratory Directed Research and Development Program (project 32112192) and by DOE's Office of Basic Energy Sciences, Division of Chemical Sciences, Geosciences and Biosciences. Oak Ridge National Laboratory (ORNL) is managed by UT-Battelle, LLC for the US Department of Energy under Contract No. DE-AC05-00OR22725. Certain commercial equipment, instruments, instruments, or materials are identified in this paper to foster understanding. Such identification does not imply recommendation or endorsement by the National Institute of Standards and Technology, nor does it imply that the materials or equipment identified are necessarily the best available for the purpose.

References

- [1] H. Ohtaki, T. Radnai, Chem. Rev. 93 (1993) 1157 and references therein.
- [2] N.A. Hewish, J.E. Enderby, W.S. Howells, J. Phys. C: Solid State Phys. 16 (1983) 1777.
- [3] P.S. Salmon, J. Phys. C: Solid State Phys. 20 (1987) 1573.

- [4] J.C. Lassegues, D. Cavagnat, *Mol. Phys.* 68 (1989) 803.
- [5] D. Cavagnat, J.C. Lassegues, *Sol. State Ionics* 46 (1991) 11.
- [6] T.V. Karmazina, A.A. Kavitskaya, V.I. Slisenko, A.A. Petrachkov, A.A. Vasilkevich, *Desalination* 184 (2005) 337 and references therein.
- [7] E. Mamontov, D.R. Cole, *Phys. Chem. Chem. Phys.* 8 (2006) 4908.
- [8] For example: J.-F. Dufreche, O. Bernard, P. Turq, A. Mukherjee, B. Bagchi, *Phys. Rev. Lett.* 88 (2002) 095902.
- [9] I. Ichinose, H. Senzu, T. Kunitake, *Chem. Mater.* 9 (1997) 1296.
- [10] W.F. Yan, B. Chen, S.M. Mahurin, E.W. Hagaman, S. Dai, S.H. Overbury, *J. Phys. Chem. B* 108 (2004) 2793.
- [11] W.F. Yan, S.M. Mahurin, S.H. Overbury, S. Dai, *Chem. Mater.* 17 (2005) 1923.
- [12] W.F. Yan, S.M. Mahurin, Z.W. Pan, S.H. Overbury, S. Dai, *J. Am. Chem. Soc.* 127 (2005) 10480.
- [13] P.Y. Feng, X.H. Bu, G.D. Stucky, D.J. Pine, *J. Am. Chem. Soc.* 122 (2000) 994.
- [14] J.C. Groen, L.A.A. Peffer, J. Perez-Ramirez, *Micropor. Mesopor. Mater.* 60 (2003) 1.
- [15] A. Meyer, R.M. Dimeo, P.M. Gehring, D.A. Neumann, *Rev. Sci. Instrum.* 74 (2003) 2759.
- [16] T. Takamuku, M. Yamagami, H. Wakita, Y. Masuda, T. Yamaguchi, *J. Phys. Chem. B* 101 (1997) 5730.
- [17] D.C. Steytler, J.C. Dore, C.J. Wright, *J. Phys. Chem.* 87 (1983) 2458.
- [18] S. Takahara, M. Nakano, S. Kittaka, Y. Kuroda, T. Mori, H. Hamano, T. Yamaguchi, *J. Phys. Chem. B* 103 (1999) 5814.
- [19] K. Morishige, K. Nobuoka, *J. Chem. Phys.* 107 (1997) 6965.
- [20] M.-C. Bellissent-Funel, J. Lal, L. Bosio, *J. Chem. Phys.* 98 (1993) 4246.
- [21] Y.-G. Zhang, J.D. Frantz, *Chem. Geol.* 74 (1989) 289.
- [22] J.T. Cabral, A. Luzar, J. Teixeira, M.-C. Bellissent-Funel, *J. Chem. Phys.* 113 (2000) 8736.
- [23] H.N. Bordallo, K.W. Herwig, B.M. Luther, N.E. Levinger, *J. Chem. Phys.* 121 (2004) 12457.
- [24] D. Russo, R.K. Murarka, G. Hura, E.R. Verschell, J.R.D. Copley, T. Head-Gordon, *J. Phys. Chem. B* 108 (2004) 19885.
- [25] D. Russo, G. Hura, T. Head-Gordon, *Biophys. J.* 86 (2004) 1852.
- [26] D. Russo, R.K. Murarka, J.R.D. Copley, T. Head-Gordon, *J. Phys. Chem. B* 109 (2005) 12966.
- [27] C. Malardier-Jugroot, T. Head-Gordon, *Phys. Chem. Chem. Phys.* 9 (2007) 1962.
- [28] N. Sahai, K.M. Rosso, in: J. Lützenkirchen (Ed.), *Surface Complexation Modeling*, 2006, p. 359.
- [29] Z. Zhang, P. Fenter, N.C. Sturchio, M.J. Bedzyk, M.L. Machesky, D.J. Wesolowski, *Surf. Sci.* 601 (2007) 1129.
- [30] Z. Zhang, P. Fenter, L. Cheng, N.C. Sturchio, M.J. Bedzyk, M.L. Machesky, L.M. Anowitz, D.J. Wesolowski, *J. Colloid Interface Sci.* 295 (2006) 50.
- [31] S.S. Lee, K.L. Nagy, P. Fenter, *Geochim. Cosmochim. Acta* 71 (2007) 5763.
- [32] A. Faraone, L. Liu, C.-Y. Mou, C.-W. Yen, S.-H. Chen, *J. Chem. Phys.* 121 (2004) 10843.
- [33] L. Liu, A. Faraone, C.-Y. Mou, C.-W. Yen, S.-H. Chen, *J. Phys.: Condens. Matter* 16 (2004) S5403.
- [34] E. Mamontov, *J. Chem. Phys.* 123 (2005) 171101.
- [35] E. Mamontov, C.J. Burnham, S.-H. Chen, A.P. Moravsky, C.-K. Loong, N.R. de Souza, A.I. Kolesnikov, *J. Chem. Phys.* 124 (2006) 194703.
- [36] S.-H. Chen, L. Liu, E. Fratini, P. Baglioni, A. Faraone, E. Mamontov, *Proc. Nat. Acad. Sci.* 103 (2006) 9012.
- [37] S.-H. Chen, L. Liu, X.-Q. Chu, Y. Zhang, E. Fratini, P. Baglioni, A. Faraone, E. Mamontov, *J. Chem. Phys.* 125 (2006) 171103.
- [38] E. Mamontov, L. Vlack, D.J. Wesolowski, P.T. Cummings, W. Wang, L.M. Anovitz, J. Rosenqvist, C.M. Brown, V. Garcia Sakai, *J. Phys. Chem. C* 111 (2007) 4328.
- [39] X.-Q. Chu, A.I. Kolesnikov, A.P. Moravsky, V. Garcia-Sakai, S.-H. Chen, *Phys. Rev. E* 76 (2007) 021505.
- [40] L. Xu, P. Kumar, S.V. Buldyrev, S.-H. Chen, P.H. Poole, F. Sciortino, H.E. Stanley, *Proc. Nat. Acad. Sci.* 102 (2005) 16558.
- [41] K. Ito, C.T. Moynihan, C.A. Angell, *Nature (London)* 398 (1999) 492.
- [42] J. Swenson, *Phys. Rev. Lett.* 97 (2006) 89801; S. Cerveny, J. Colmenero, A. Alegria, *Phys. Rev. Lett.* 97 (2006) 189802; S.-H. Chen, L. Liu, A. Faraone, *Phys. Rev. Lett.* 97 (2006) 189803.
- [43] J. Teixeira, A. Luzar, S. Longeville, *J. Phys.: Condens. Matter* 18 (2006) S2353.
- [44] D.E. Moilanen, N.E. Levinger, D.B. Spry, M. D.M.D. Fayer, *J. Am. Chem. Soc.* 129 (2007) 14311.
- [45] V. Garbuio, C. Andeani, S. Imberti, A. Pietropaolo, G.F. Reiter, R. Senesi, M.A. Ricci, *J. Chem. Phys.* 127 (2007) 154501.
- [46] A. Paciaroni, S. Cinelli, G. Onori, *Biophys. J.* 83 (2002) 1157.
- [47] K. Wood, M. Plazanet, F. Gabel, B. Kessler, D. Oesterhelt, D.J. Tobias, G. Zaccai, M. Weik, *Proc. Nat. Acad. Sci.* 104 (2007) 18049.
- [48] A.A. Levchenko, A.I. Kolesnikov, N.L. Ross, J. Boerio-Goates, B.F. Woodfield, G. Li, A. Navrotsky, *J. Phys. Chem. A* 111 (2007) 12584.